JMEPEG (2001) 10:731–739

Hot Deformation Mechanisms in Ti-5.5Al-1Fe Alloy

V.V. Balasubrahmanyam and Y.V.R.K. Prasad

(Submitted 12 March 2001)

The mechanisms of hot deformation in the alloy Ti-5.5Al-1Fe have been studied in the temperature range 750 to 1150 °C and with the true strain rate varying from 0.001 to 100 s^{-1} by means of isothermal compression tests. At temperatures below β transus and low strain rates, the alloy exhibited steady-state flow behavior, while, at high strain rates, either continuous flow softening or work hardening followed by flow softening was observed. In the β region, the deformation behavior is characterized by steady-state behavior at low strain rates, yield drops at intermediate strain rates, and oscillations at high strain rates. The processing maps revealed two domains. (1) In the temperature range 750 to 1050 °C and at strain rates lower than 0.01 s^{-1}, the material exhibits fine-grained superplasticity. The apparent activation energy for superplastic deformation is estimated to be about 328 kJ/mole. The optimum conditions for superplasticity are 825 °C and 0.001 s^{-1}. (2) In the β region, a domain occurs at temperatures above 1100 °C and at strain rates from 0.001 to 0.1 s^{-1} with its peak efficiency of 47% occurring at 1150 °C and 0.01 s^{1}. On the basis of kinetic analysis, tensile ductility, and grain size variation, this domain is interpreted to represent dynamic recrystallization (DRX) of β phase. The apparent activation energy for DRX is estimated to be 238 kJ/mole. The grain size (d) is linearly dependent on the Zener-Hollomon parameter (Z) per the equation

$$\log (d) = 2.86 - 0.023 \log (Z)$$

In the regimes in the temperature range 750 to 825 °C and at strain rates from 0.01 to 1.2 s^{-1} and at temperatures above 1050 °C and strain rates above 10 s^{-1}, the material exhibits flow instabilities manifested in the form of adiabatic shear bands.

Keywords deformation mechanisms, hot working, Ti-5.5Al-1Fe alloy

1. Introduction

Ti-Al-Fe alloys are being considered as implant materials owing to their high strength-to-weight ratio, low elastic modulus, corrosion resistance, and good tissue tolerance. Unlike the most commonly used alloy, Ti-6Al-4V,[1] these alloys do not cause biotoxicity due to the absence of vanadium.[2] Iron, on the other hand, is nontoxic and its diffusion coefficient is two orders of magnitude higher than that of Ti or V imparting better hot workability. Two alloys are developed on the basis of a Ti-Al-Fe system, *viz.* Ti-5.5Al-2Fe and Ti-5.5Al-1Fe, and these alloys have mechanical properties comparable to that of Ti-6Al-4V.[3–5] The alloy Ti-5.5Al-1Fe has the same β transus and M_s temperature as Ti-6Al-4V.[3]

Koike *et al.*[6] reported that the alloy Ti-5.5Al-1Fe exhibits superplasticity like its counterpart Ti-6Al-4V over wide ranges of temperature from 777 to 927 °C and strain rates 10^{-4} to 10^{-2} s^{-1}. The volume fraction of the β phase increases during superplastic deformation[7] and is caused by the occurrence of a stress-induced transformation.[8]

The above studies on hot deformation are confined to a limited range of temperatures in the ($\alpha + \beta$) field in which the superplastic deformation dominates. However, many industrial forming processes encompass wider temperature and strain rate ranges, and it is important to understand the deformation mechanisms occurring during hot working of the alloy in order to optimize the hot workability and to achieve microstructural control. Thus, the objective of the present investigation is to characterize the hot deformation behavior of Ti-5.5Al-1Fe alloy over a temperature that covers ($\alpha + \beta$) as well as β phase fields and strain rates corresponding to those of industrial machinery.

V.V. Balasubrahmanyam and **Y.V.R.K. Prasad,** Department of Metallurgy, Indian Institute of Science, Bangalore 560012, India. Contact e-mail: yprasad@metalrg.iisc.ernet.in.

2. Experimental

2.1 Material

The Ti-Al-Fe alloy having Al-5.84, Fe-1.48, O-0.16, and Ti-bal., by wt.%, was used in the present study. The starting material was in the form of a rod of 25 mm diameter, produced by hot rolling in the ($\alpha + \beta$) phase field. The initial microstructures of the alloy in the longitudinal and transverse directions are shown in Fig. 1(a) and (b), respectively. It can be seen that the microstructure consists of slightly elongated α grains (Fig. 1a) with about 15% of β phase. The transverse section exhibits near-equiaxed ($\alpha + \beta$) structure typical of a material processed in the ($\alpha + \beta$) range. The β transus of the alloy is about 1050 °C.

2.2 Hot Compression Testing

Cylindrical specimens of 15 mm height and 10 mm diameter were machined for compression testing in the ($\alpha + \beta$) regime, while larger specimens of 22.5 mm height and 15 mm diameter were used to obtain an accurate measurement of flow stress in the β range. Concentric grooves of 0.5 mm depth were provided on the top and bottom faces of the specimen for effective

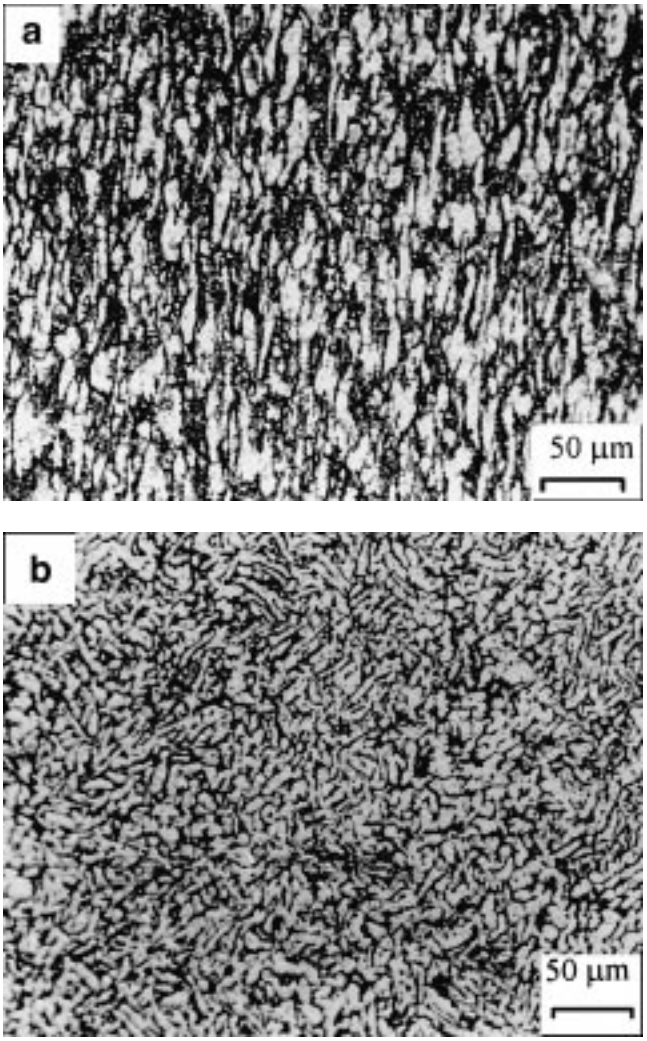

Fig. 1 Initial microstructure of Ti-5.5Al-1Fe alloy in the as-received condition: (**a**) longitudinal section and (**b**) transverse section. The rolling direction is vertical

lubrication during testing. The edges of the specimen were chamfered to avoid foldover during the initial stages of testing. The temperature of the specimen during the test was monitored within an accuracy of ±2 °C by means of a fine thermocouple introduced into a small hole of 0.8 mm diameter at half the height of the specimen. This also helps in measurement of adiabatic temperature rise during the testing.

Compression tests were carried out in a temperature range of 750 to 1150 °C at an interval of 50 °C and at true strain rates of 0.001 to 100 s^{-1}. The specimens were coated with a thick layer of Delta Glaze glass lubricant (Acheson Industries, Port Huron, MI), which is melted at test temperatures and gives a protection layer on the sample. The alpha layer on the surface was very thin, which indicates that the glass layer is effective in reducing the oxidation of the surface. The specimens were held at the test temperature for 10 min before commencement of the test to obtain an equiaxed structure. Platens made of IN100 (International Nickel, Huntington, WV) were used for testing up to 1050 °C, and special ceramic inserts were used for testing at 1100 and 1150 °C. The specimens were deformed to half the original height in each case (true strain of about 0.7) and were air cooled after deformation. Deformed specimens were sectioned parallel to the compression axis and prepared for metallographic examination using standard techniques. The specimens were etched with a solution of 5 mL HF, 5 mL HNO_3, in 100 mL of water.

2.3 Hot Tensile Testing

Cylindrical specimens of 25 mm gage length and 4 mm diameter were used for tensile testing. Hot tensile tests were conducted in the temperature range 1000 to 1150 °C at a nominal strain rate of 0.01 s^{-1} with a constant actuator speed of 0.25 mm per second. The tensile tests were carried out to fracture by taking appropriate precautions to prevent oxidation in a manner described above, and the total elongation as a function of temperature was recorded.

3. Results and Discussion

The constitutive behavior of the material can be understood from the analysis of stress-strain curves,[9] kinetic analysis,[10] and processing maps.[11] The load stroke data obtained on the compression specimens were processed by means of a computer program developed for the purpose to obtain true stress-true plastic strain curves.

3.1 Stress-Strain Behavior

The stress strain curves obtained at two temperatures 850 °C in the ($\alpha + \beta$) phase field and 1100 °C in the β phase field are shown in Fig. 2(a) and (b), respectively. These curves are representative of the behavior of the alloy below and above the transus temperature. The curves reveal the following features.

- In the ($\alpha + \beta$) region (Fig. 2a), *e.g.*, at 850 °C and at strain rates below 0.1 s^{-1}, the flow curves are of steady-state type. At strain rates of 10 and 100 s^{-1}, there is an initial work hardening followed by flow softening. The steady-state behavior at low strain rates is suggestive of superplasticity or dynamic recrystallization. Flow softening at higher strain rates may have been caused by flow instabilities or dynamic recrystallization.
- In the β regime (Fig. 2b), *e.g.*, at 1100 °C, the flow curves below 0.1 s^{-1} exhibit steady-state behavior. The flow stresses are extremely low. On the other hand, at strain rates higher than 10 s^{-1}, the flow curves are wavy or oscillatory. The oscillations in stress strain curves are indicative of DRX or unstable deformation or cracking. All the flow curves show yield drops. The magnitude of yield drop increases with an increase in strain rate or decrease in temperature. Such yield points have been reported during hot deformation of many β titanium alloys and are considered to be a characteristic feature of β deformation.[15,16] The flow stress data as a function of temperature, strain rate, and strain are presented in Table 1.

3.2 Kinetic Analysis

Under hot working conditions, the flow stress (σ) is related to the strain rate ($\dot{\varepsilon}$) and temperature (T) through the rate equation given by

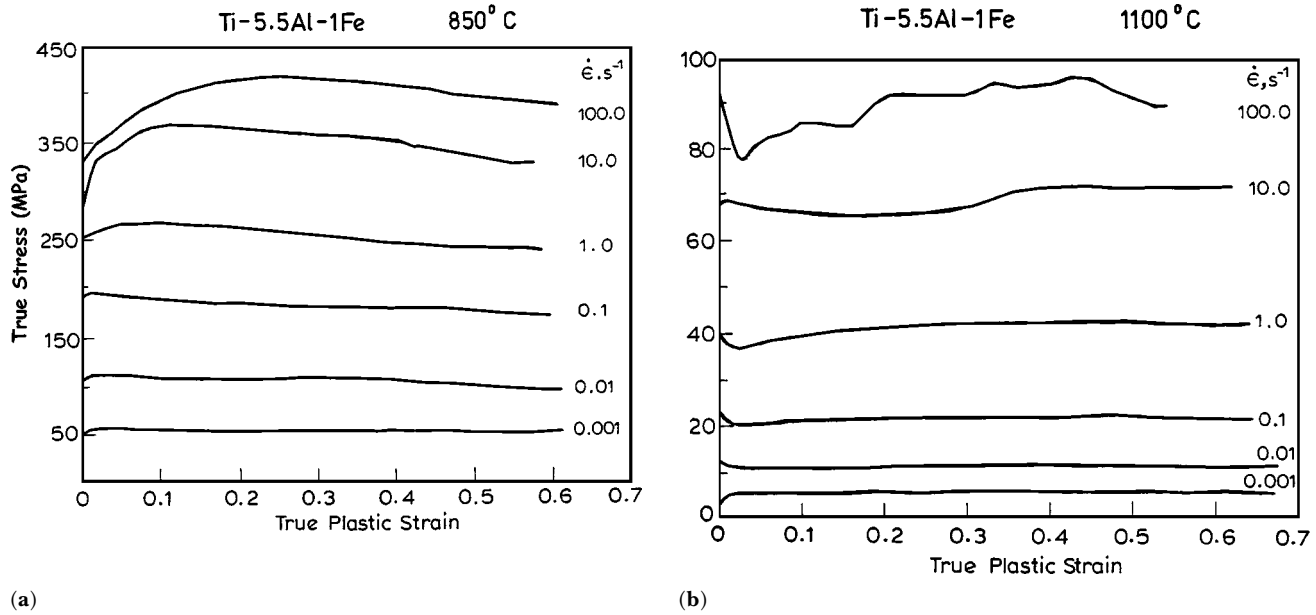

(**a**) (**b**)

Fig. 2 (**a**) True stress-true plastic strain curves obtained in the isothermal compression at 850 °C at different strain rates on the Ti-5.5Al-1Fe alloy. (**b**) True stress-true plastic strain curves obtained in isothermal compression at 1100 °C at different strain rates in the Ti-5.5Al-1Fe alloy

Table 1 Variation of flow stress (MPa) of Ti-5.5Al-1Fe alloy with temperature, strain, and strain rate (corrected for adiabatic temperature rise)

Strain	Strain rate, s^{-1}	750 °C	800 °C	850 °C	900 °C	950 °C	1000 °C	1050 °C	1100 °C	1150 °C
	0.001	124.3	80.8	56.1	30.5	23.4	16.1	6.1	5.6	4.7
	0.010	239.0	151.0	110.6	81.8	54.2	27.2	13.4	10.7	9.1
0.1	0.100	348.4	261.1	197.9	138.7	74.9	43.6	26.2	20.9	16.5
	1.000	449.8	375.7	300.6	213.4	147.1	67.1	44.3	39.8	31.1
	10.00	515.9	430.4	373.5	310.4	250.8	117.3	80.0	66.6	53.7
	100.0	548.8	479.0	426.1	394.8	280.0	155.6	102.6	86.1	69.2
	0.001	120.6	78.7	53.6	29.9	22.6	15.7	6.3	5.9	4.8
	0.010	239.1	152.2	106.8	78.9	52.2	26.2	14.0	11.2	9.2
0.2	0.100	339.0	255.3	192.5	135.2	73.7	43.6	27.2	21.1	17.0
	1.000	454.9	373.1	295.4	210.2	146.3	67.5	47.8	40.9	31.9
	10.00	533.5	436.6	371.2	299.1	242.0	113.3	80.2	65.3	54.4
	100.0	590.1	514.9	456.7	417.3	298.0	166.5	115.5	92.1	75.5
	0.001	120.1	78.7	53.9	30.1	22.6	15.8	6.6	5.9	4.2
	0.010	240.7	153.5	106.7	77.0	52.2	26.5	14.7	11.4	9.4
0.3	0.100	332.4	251.9	191.2	134.4	73.5	44.0	27.5	21.5	17.4
	1.000	437.0	361.9	287.8	205.1	144.4	66.3	47.8	42.0	33.3
	10.00	507.5	434.1	366.5	290.8	235.2	115.6	80.7	67.5	57.1
	100.0	614.8	530.3	464.4	415.1	303.5	171.9	117.3	92.1	81.4
	0.001	118.4	77.8	53.3	30.3	22.8	15.6	6.8	5.7	4.8
	0.010	240.7	152.9	104.6	75.8	51.9	26.4	14.8	11.6	9.4
0.4	0.100	326.1	249.6	189.3	134.1	72.7	44.3	27.6	21.5	17.7
	1.000	411.3	346.6	277.8	198.4	141.3	64.3	47.5	42.4	33.5
	10.00	496.1	424.0	355.7	280.1	227.3	117.0	82.5	71.4	60.6
	100.0	606.8	519.7	453.0	406.6	299.6	171.9	118.8	93.9	84.3
	0.001	115.8	75.5	51.6	30.2	22.5	15.4	6.9	5.7	4.7
	0.010	236.6	149.3	101.3	74.4	51.0	25.8	14.7	11.6	9.5
0.5	0.100	326.3	245.4	184.9	130.9	71.2	44.1	27.7	21.3	17.8
	1.000	405.3	338.5	269.9	193.3	138.6	63.0	47.9	42.2	33.7
	10.00	488.2	407.8	341.1	273.0	219.4	113.0	82.3	71.4	60.6
	100.0	604.4	510.1	440.7	399.4	291.1	168.3	117.1	90.8	84.9

$$\dot{\varepsilon} = A\sigma^n \exp\left(\frac{-Q}{RT}\right) \qquad \text{(Eq 1)}$$

where A and n are constants, and Q is the activation energy for hot working.

The kinetic parameters n and Q are evaluated for Ti-5.5Al-1Fe alloy using the flow stress data at a strain of 0.5 (Table 1) as a function of stain rate and temperature. The variation of

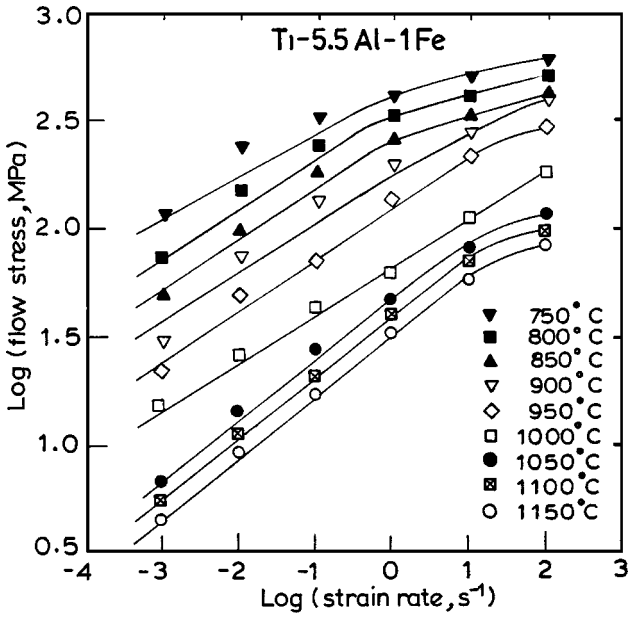

Fig. 3 Variation of flow stress with strain rate at different temperatures for Ti-5.5Al-1Fe alloy

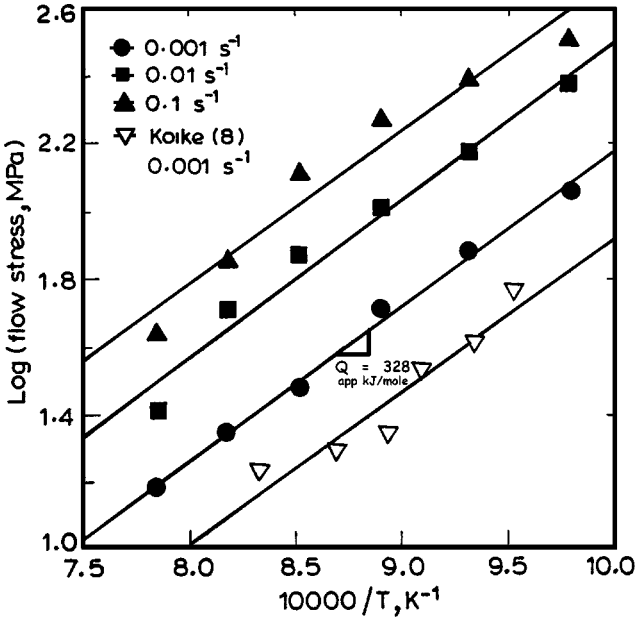

Fig. 4 Arrhenius plot showing the variation of flow stress with temperature at different strain rates in the (α + β) region of Ti-5.5Al-1Fe alloy

flow stress with strain rate is shown in Fig. 3. The inverse of slope gives the stress exponent *n* in Eq 1. It can be seen that *n* is strain rate dependent, although, over a limited range of strain rates, it may be considered to be a constant. In the two-phase region (750 to 1000 °C) and in the strain rate range (0.001 to 0.1 s^{-1}), the value of the stress exponent is in the range of 3.77 to 3.85. The Arrhenius plot for estimating the apparent activation energy for deformation in the (α + β) region is shown in Fig. 4. The data from Koike *et al.*[8] on T-5.5Al-1Fe are also plotted for comparison. It can be said that the data fit is very good at strain rates lower than 0.01 s^{-1}, but the data at the higher strain rate of 0.1 s^{-1} deviate from the straight-line relationship at lower and higher temperatures. The apparent activation energy estimated from the plot is about 328 kJ/mole and compares very well with the value of 314 kJ/mole obtained by Koike *et al.*[6] The estimated apparent activation energy is much higher than that for self-diffusion of βTi (153 kJ/mole)[17] or alloying elements such as Al (92 to 107 kJ/mole), V (135 kJ/mole), or Fe (132 kJ/mole) in titanium.[18–20]

The analysis of flow stress data in the β region gives a value of 3.6 for *n*, and the corresponding Arrhenius plot is shown in Fig. 5. It can be seen that the data fit very well into a straight line at all strain rates. The apparent activation energy is estimated to be 238 kJ/mole, which is slightly higher than the value of 210 kJ/mole for Ti-6Al-4V during β deformation.[21] It is reported[22] that the activation energy for β deformation of many α titanium alloys is in the range 180 to 220 kJ/mole and that for hot deformation of β alloys is 130 to 175 kJ/mole.[15]

The kinetic analysis is carried out further to take into account the combined effect of temperature and strain rate in terms of the Zener-Hollomon parameter given by

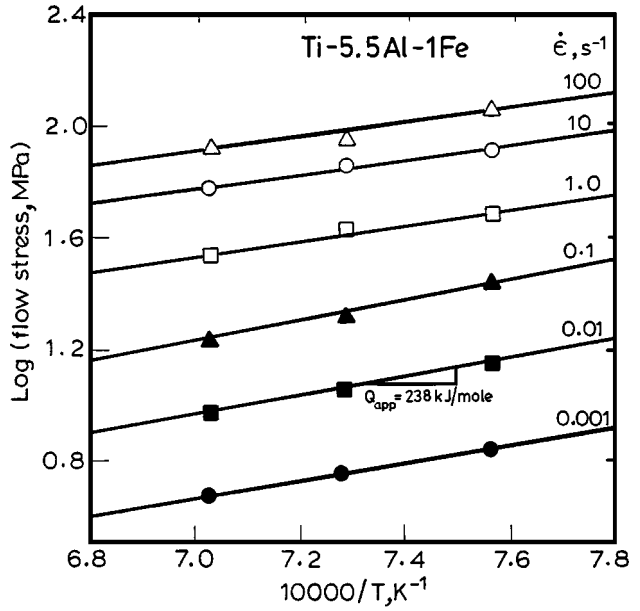

Fig. 5 Arrhenius plot showing the variation of flow stress with temperature at different strain rates in the β region of Ti-5.5Al-1Fe alloy

$$Z = \dot{\varepsilon}\, e\, \frac{Q}{RT} \qquad \text{(Eq 2)}$$

The parameter is plotted as a function of flow stress and is shown in Fig. 6(a) and (b) for the (α + β) and β phase fields, respectively. The plots exhibit an excellent linear relationship, and thus, it can be concluded that the kinetic rate equation is obeyed in a limited strain rate range of 0.001 to 0.1 s^{-1} in the (α + β) region and 0.001 to 0.1 s^{-1} in the β phase field.

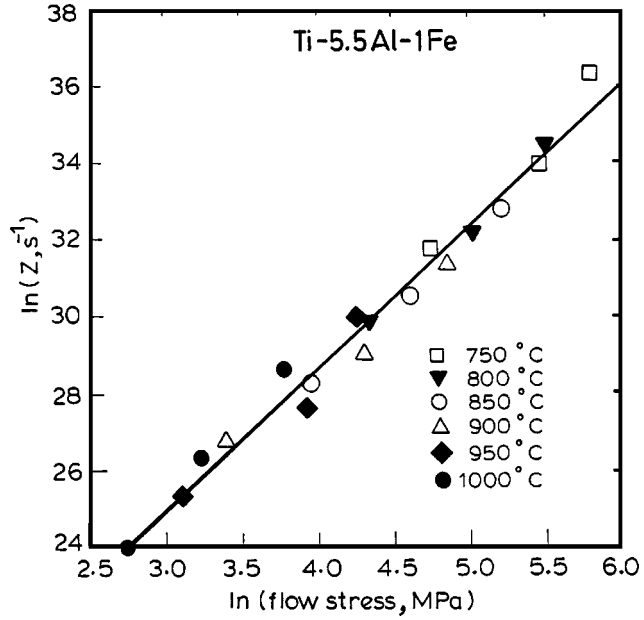

(**a**)

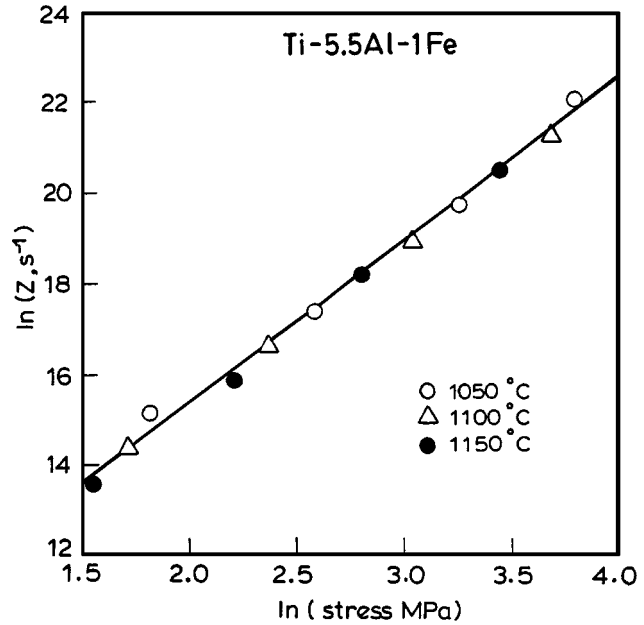

(**b**)

Fig. 6 (**a**) Variation of flow stress with Zener-Hollomon parameter in the ($\alpha + \beta$) region. (**b**) Variation of flow stress with Zener-Hollomon parameter in the β phase field

3.3 Processing Maps

Processing maps describe the manner in which power is dissipated through microstructural changes during hot deformation and are very useful in explaining the hot deformation behavior consistently for a large number of metals and alloys.[12,13] The processing map consists of superposition of the power dissipation map and instability map developed in temperature strain rate space. The power dissipation map is a three-dimensional variation of the efficiency of power dissipation η as a function of strain rate and temperature. The dimensionless parameter η is obtained by comparing the dissipation in the workpiece with that of a linear dissipator and is given by

$$\eta = \frac{2m}{m + 1} \qquad \text{(Eq 3)}$$

where m is the strain rate sensitivity of flow stress. The processing map is generally obtained as a two-dimensional isoefficiency contour map in the temperature-strain rate frame. The contours represent the rate of metallurgical processes. A continuum instability criterion has been developed based on the principle of irreversible thermodynamics applied to large plastic flow[14] and is given by

$$\xi(\dot{\varepsilon}) = \frac{\partial \ln (m/m + 1)}{\partial \ln \dot{\varepsilon}} + m < 0 \qquad \text{(Eq 4)}$$

where $\xi(\dot{\varepsilon})$ is a dimensionless instability parameter and $\dot{\varepsilon}$ is the strain rate. Flow instabilities occur when the parameter $\eta(\dot{\varepsilon})$ becomes negative. This parameter is plotted against temperature and strain rate to obtain an instability map. Thus, the processing maps exhibit domains in which specific microstructural mechanisms operate as well as regimes where flow instabilities such as adiabatic shear bands or flow localization will occur.

A cubic spline fit between log σ and log $\dot{\varepsilon}$ was used to obtain strain rate sensitivity over finer intervals of strain rates and temperatures. The efficiency of power dissipation η was then calculated as a function of temperature and strain rate using Eq 3 and plotted as an isoefficiency contour map. The data were also used to evaluate the instability parameter by means of Eq 4 as a function of temperature and strain rate to obtain an instability map.

The processing maps generated per the procedure described in Section 2.3 at strains of 0.3 and 0.5 are shown in Fig. 7(a) and (b), respectively. The maps at both strains exhibit similar features, indicating that the strain effect is not significant. The maps reveal two domains, as described below.

Domain 1 occurs in the ($\alpha + \beta$) region from 750 °C to the β transus temperature (~1050 °C) and in the lower strain rate range of 0.001 to 0.01 s^{-1}. The peak efficiency value is relatively high and the strain rate sensitivity is 0.4, indicating that this could be a domain of superplastic deformation. The maximum value of efficiency is 57% and occurs at 825 °C and 0.001 s^{-1}.

The ductility data obtained by Koike *et al.*[6] in the temperature range 777 to 927 °C and with a strain rate of 0.001 s^{-1} for the Ti-5.5Al-1Fe alloy is shown in Fig. 8(a), and the efficiency variation at 0.001 s^{-1} obtained from the map (Fig. 7b) is shown in Fig. 8(b) for the purpose of comparison. An abnormally high value of about 800% elongation is obtained at a temperature of 827 °C, at which efficiency is also maximum. Thus, the temperature for peak efficiency is the optimum for the occurrence of superplasticity. The microstructures obtained on the specimens deformed at temperatures of 750, 850, and 950 °C are shown in Fig. 9(a) to (c). From the microstructures, it is observed that α grain size is fine (~16 μm) and remained nearly unchanged in the temperature range considered. Therefore, it can be inferred that the mechanism controlling the hot deformation in domain 1 is superplasticity. The estimated apparent

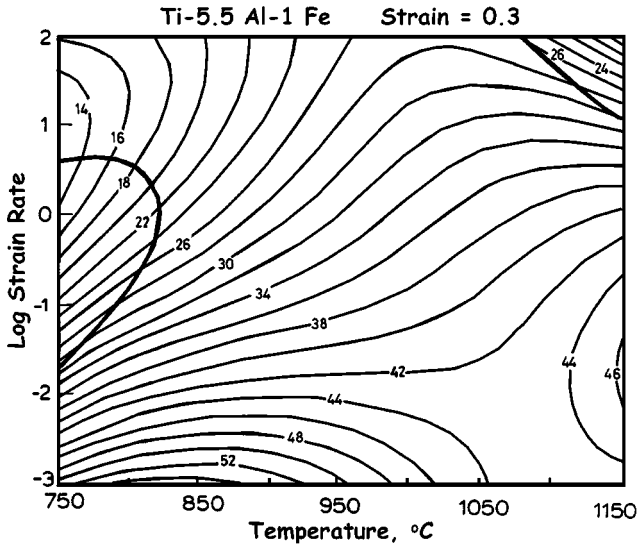

(**a**)

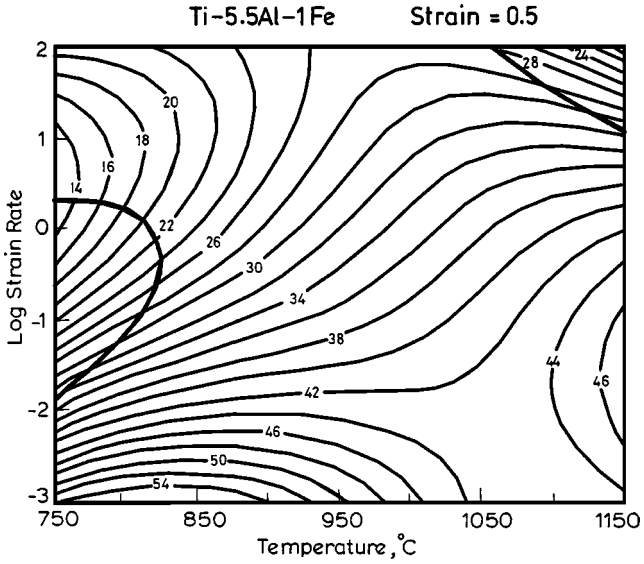

(**b**)

Fig. 7 (**a**) Processing map for Ti-5.5Al-1Fe alloy at a strain of 0.3. The numbers against the contours represent the efficiency of power dissipation expressed in percent. The thick lines represent the boundaries of the instability regimes. (**b**) Processing map for Ti-5.5Al-1Fe alloy at a strain of 0.5. The numbers against the contours represent the efficiency of power dissipation expressed in percent. The thick lines represent the boundaries of the instability regimes

activation energy of 328 kJ/mole from kinetic analysis is much higher than that for the self-diffusion of βTi or that of alloying elements. It is proposed by Koike *et al.*[8] that stress-induced transformation to β accommodates the stress concentration developed during grain boundary sliding in superplastic deformation. This takes place in two stages. In the initial stages of deformation, agglomeration of β phase occurs on grain boundaries perpendicular to the tensile axis, during which volume fraction of β does not significantly change. At strains higher than about 200%, the stress concentration at the depleted grain

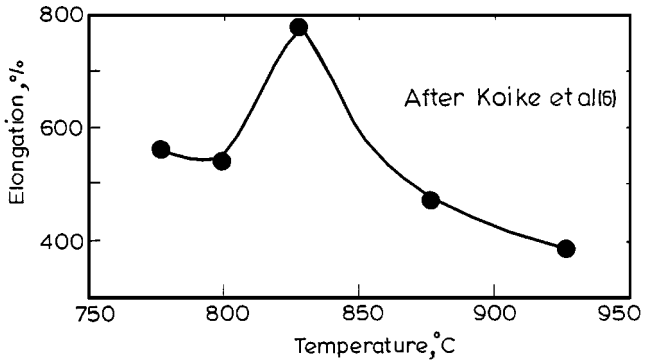

(**a**)

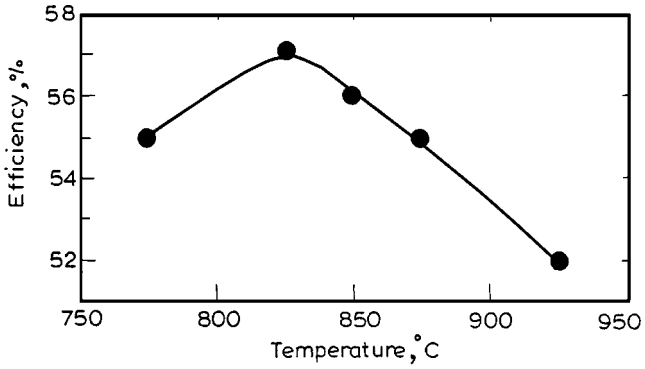

(**b**)

Fig. 8 Variation of (**a**) tensile ductility and (**b**) efficiency with temperature in the superplasticity domain of Ti-5.5Al-1Fe alloy

boundaries leads to the transformation of α to β phase with a concomitant increase in the volume fraction of β. However, in the present study, the total strains involved are only about 50%, and so it is not likely that they would result in a significant change in the β volume fraction. This is supported by the observations that the maps are unchanged with strain as are the deformed microstructures.

Domain 2 appears in the β phase field in the temperature range 1100 to 1150 °C and in the strain rate range 0.001 to 0.1 s^{-1} with a peak efficiency of about 47% at 1150 °C/0.01 s^{-1}. The domain does not appear to have fully developed and may extend beyond 1150 °C. In order to establish the mechanism responsible for deformation under the conditions conforming to domain 2, the microstructures of the specimens deformed at 1100 and 1150 °C and 0.001 and 0.1 s^{-1} have been observed. These are shown in Fig. 10(a) to (c). Cooling from a temperature above the transus results in the transformation of β phase, and prior β grain boundaries are delineated by grain boundary α. Due to this, the microstructural details of the specimens deformed at high temperature are somewhat masked by phase transformation. However, the prior β grain size is measured and its variation with temperature at a strain rate of 0.01 s^{-1} is shown in Fig. 11(a). The grain size increases with temperature starting from 1050 °C. Hot ductility tests were conducted on cylindrical specimens at a nominal strain rate of 0.01 s^{-1} at temperatures across the domain and are shown in Fig. 11(b). The percentage elongation initially dropped from 92% at 1050 °C to about 72% at 1100 °C before increasing to 87% at 1150

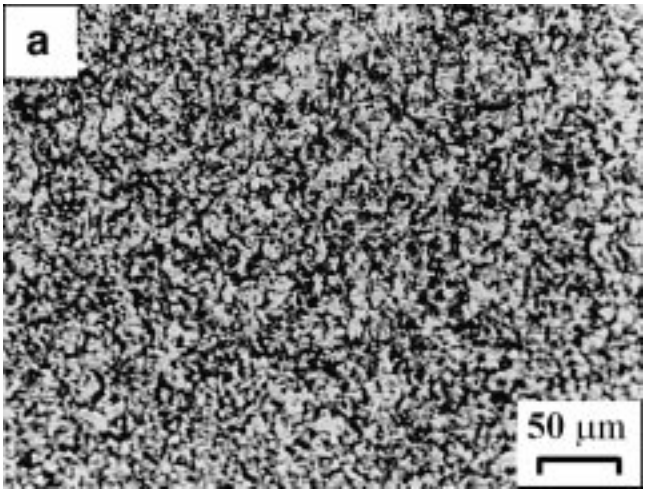

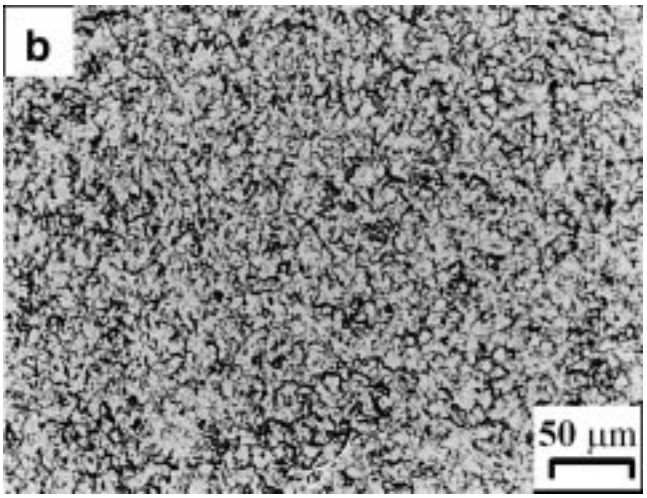

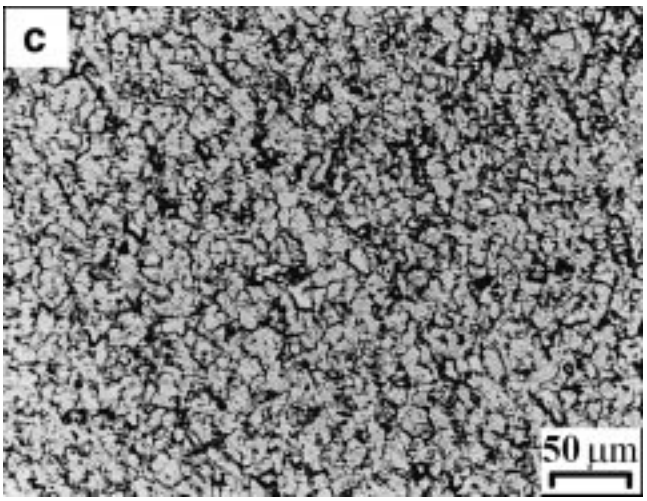

Fig. 9 Microstructures of the specimens deformed in compression at 0.001 s^{-1} at (**a**) 750 °C, (**b**) 850 °C, and (**c**) 950 °C

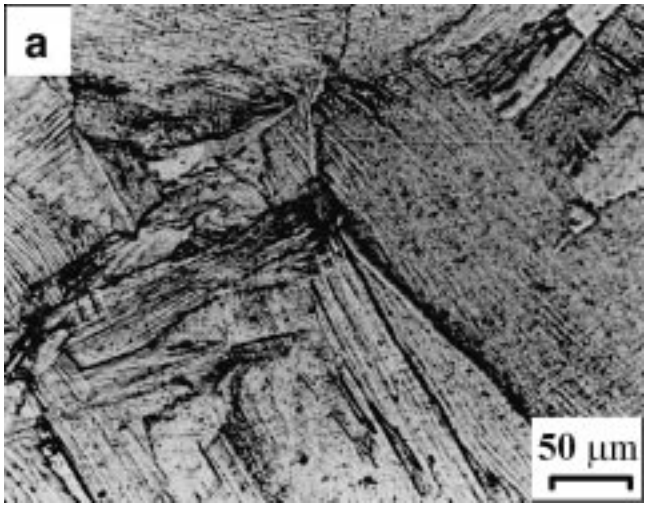

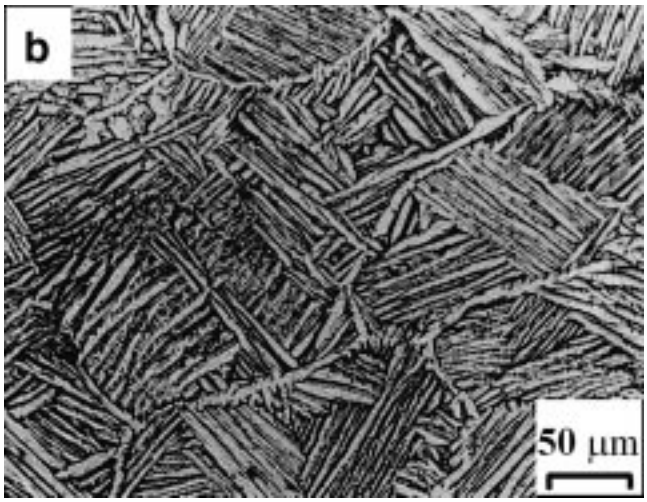

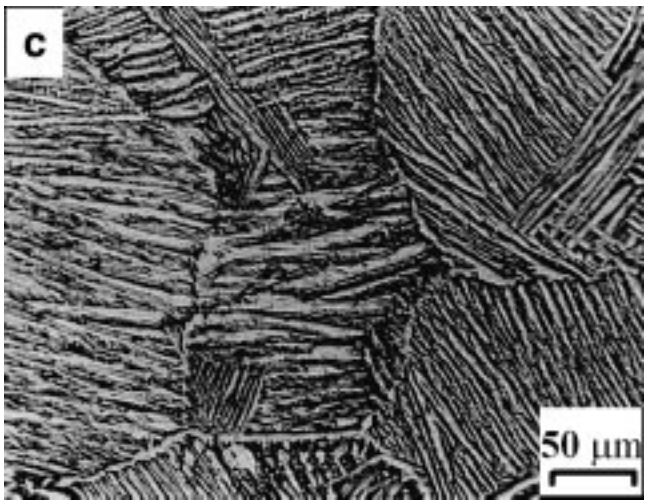

Fig. 10 Microstructures of the specimens in the β DRX domain: (**a**) 1100 °C/0.001 s^{-1}, (**b**) 1150 °C/0.01 s^{-1}, and (**c**) 1150 °C/0.1 s^{-1}

°C. The efficiency variation with temperature at 0.01 s^{-1} is shown in Fig. 11(c), which is similar to that of grain size variation (Fig. 11a). Since the domain appeared from 1100 °C only, the grain size, ductility, and efficiency exhibited an increase with temperature and are likely to increase further with temperature beyond 1150 °C. The magnitude of tensile ductility (87%) and the value peak efficiency (46%) are indicative of a DRX process, as obtained in other studies.[21] The grain size

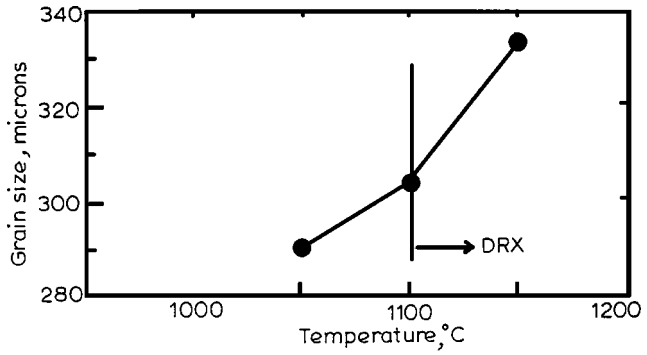

(a)

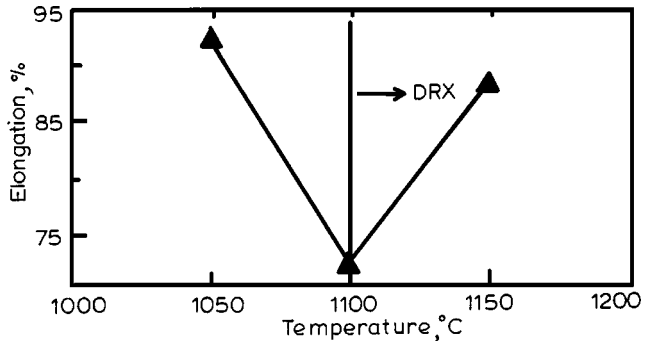

(b)

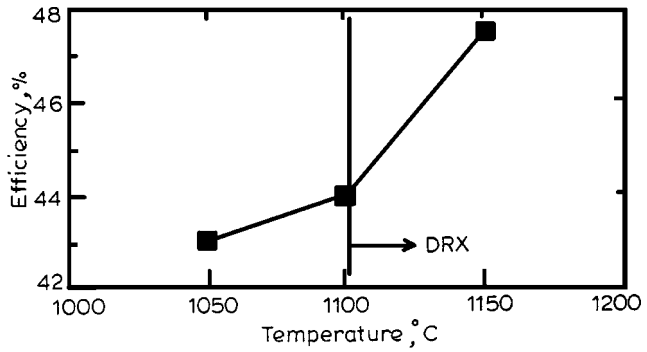

(c)

Fig. 11 Variation of (**a**) grain size, (**b**) tensile elongation, and (**c**) efficiency with temperature in the DRX domain

variation with temperature-compensated strain rate parameter Z is shown in Fig. 12. The data fits well into a straight line and the β grain size can be related to the Zener-Hollomon parameter by the equation

$$\log (d) = 2.86 - 0.023 \log (Z) \qquad \text{(Eq 5)}$$

The instability criterion given by Eq 4 predicts two regions of flow instability as shown within the areas enclosed by thick lines in the processing maps (Fig. 7a and b). The first regime is at lower temperatures and strain rates ranging from 750 to 825 °C and 0.01 to 1.2 s^{-1}, and the second one is at higher temperatures above 1050 °C and at strain rates higher than 10 s^{-1}. Further micro- and macrostructural studies are carried out

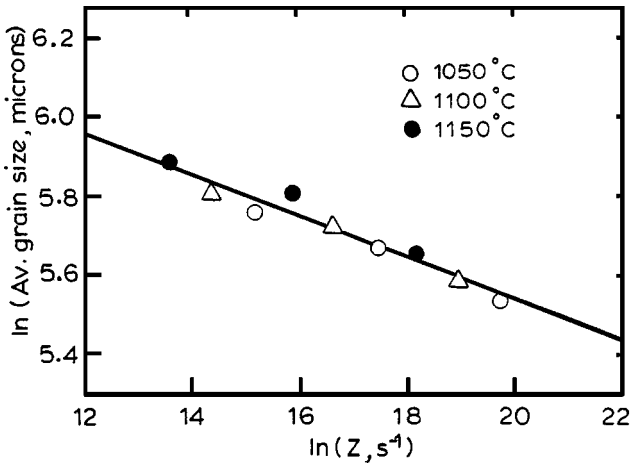

Fig. 12 Variation of grain size with Zener-Hollomon parameter in the DRX domain of Ti-5.5Al-1Fe.

to understand the manifestation of the instabilities. The macrophotographs of the specimens deformed at 750 °C at strain rates of 0.1 and 1 s^{-1} and 800 °C at 1 s^{-1} are shown in Fig. 13(a) to (c), respectively. These exhibit flow localization shear bands at about 45° to the compression axis. It can be seen that the bands become less intense with increasing temperature and decreasing stain rate. The microstructures of the specimens deformed at high temperatures of 1100 and 1150 °C and 100 s^{-1} were observed, but instabilities could not be recorded since the phase transformations associated with cooling masked the features. However, the oscillations exhibited by stress-stain curves are suggestive of flow instabilities in the β phase field.

4. Conclusions

Hot deformation behavior of the alloy Ti-5.5Al-1Fe has been characterized in the as-received condition by means of isothermal hot compression tests in the temperature range of 750 to 1150 °C and strain rates from 0.001 to 100 s^{-1}. The following conclusions are drawn from the study.

- The material exhibits fine-grained superplasticity in the temperature range from 750 to 1050 °C and strain rates below 0.01 s^{-1}. Maximum ductility occurs at 825 °C and 0.001 s^{-1}, at which the strain rate sensitivity is about 0.4. The apparent activation energy for the superplastic deformation is about 328 kJ/mole, which is higher than that for the diffusional processes.
- The β phase undergoes DRX at temperatures above 1100 °C, the optimum conditions being 1150 °C and 0.01 s^{-1}. The apparent activation energy for the β DRX is 238 kJ/mole.
- The material exhibits two regimes of flow instability: 750 to 825 °C and 0.01 to 1.2 s^{-1}; and temperatures above 1050 °C and strain rates from 10 to 100 s^{-1}. In the former regime, shear localization occurs, while in the latter, the stress-strain curves exhibit oscillations.

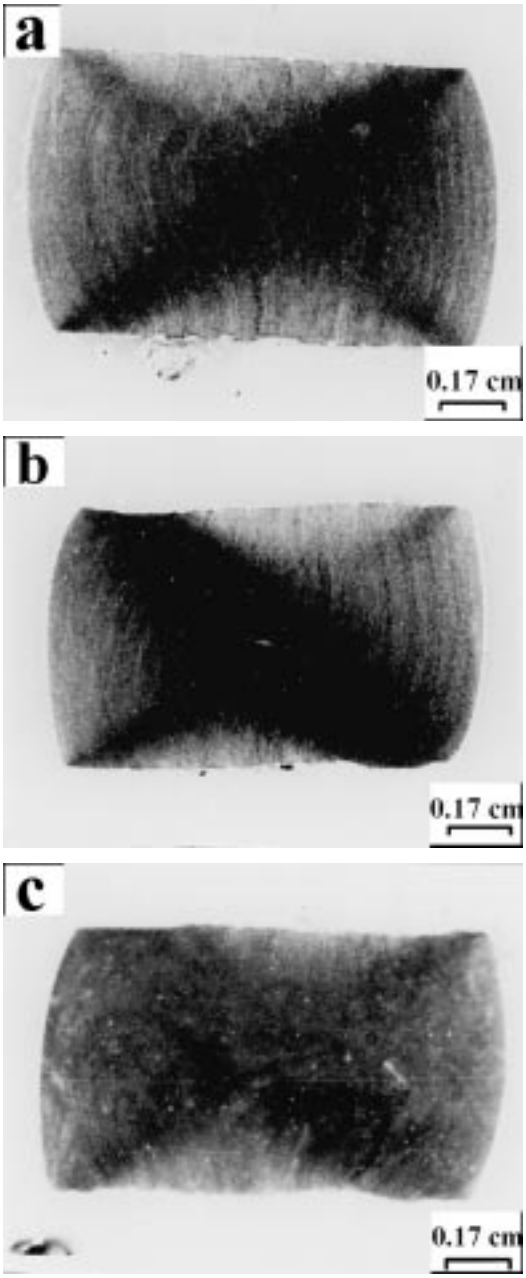

Fig. 13 Macrographs of specimens deformed (**a**) at 750 °C/0.1 s^{-1}, (**b**) at 750 °C/1 s^{-1}, and (**c**) 800 °C/1 s^{-1} showing adiabatic shear bands. The compression axis is vertical

Acknowledgments

The authors thank Messrs. S. Sasidhara and R. Ravi, Department of Metallurgy, Indian Institute of Science, Bangalore, for their help with conducting the experiments and with the computational work.

References

1. K. Wang: *Mater. Sci. Eng.,* 1996, vol. A213, pp. 134-37.
2. Y. Okazaki, Y. Ito, A. Ito, and T. Tateishi: in *Metallurgy and Technology of Practical Titanium Alloys,* S. Fujishiro, D. Eylon, and T. Kishi, eds., TMS, Warrendale, PA, 1994, pp. 313-21.
3. H. Fuji, K. Takashahi, and S. Soeda: in *Titanium '95 Science and Technology,* P.A. Blenkinsop, W.J. Evans, and H.M. Flower, eds., Institute of Materials, Oxford, United Kingdom, 1996, pp. 2539-46.
4. M. Niimomi, T. Kobayashi, O. Toriama, N. Kawakami, Y. Ishida, and Y. Matsuyama: *Metall. Mater. Trans. A,* 1996, vol. 27A, pp. 3925-35.
5. H. Fuji: *Mater. Sci. Eng.,* 1998, vol. A243, pp. 103-08.
6. J. Koike, Y. Shinoyama, H. Fuji, and K. Maruyama: *Scripta Mater.,* 1998, vol. 39 (8), pp. 1009-14.
7. J. Koike, Y. Shimoyama, T. Okamura, and K. Maruyama: *Mater. Sci. Forum,* 1999, vol. 304–306, pp. 183-88.
8. J. Koike, Y. Shimoyama, L. Ohnuma, T. Okamura, R. Kainuma, K. Ishida, and K. Maruyama: *Acta Mater.,* 2000, vol. 48 (9), pp. 2059-69.
9. I. Weiss, T.H. Froes, D. Eylon, and G.E. Welsh: *Metall. Trans. A,* 1986, vol. 17A, pp. 1935-47.
10. J.J. Jonas, C.M. Sellars, and W.J. McTegart: *Metall. Rev.,* 1969, vol. 14 (1), pp. 1-24.
11. Y.V.R.K. Prasad, H.L. Gegel, S.M. Doraivelu, J.C. Malas, J.T. Morgan, K.A. Lak, and D.R. Barker: *Metall. Trans. A,* 1984, vol. 15A, pp. 1883-92.
12. Y.V.R.K. Prasad and T. Seshacharyulu: *Int. Mater. Rev.,* 1998, vol. 43 (6), pp. 243-58.
13. Y.V.R.K. Prasad and S. Sasidhara: *Hot Working Guide: A Compendium of Processing Maps,* ASM, Materials Park, OH, 1997, pp. 449-95.
14. H. Zeigler: in *Progress in Solid Mechanics,* I.N. Sneddon and R. Hill, eds., North Holland Publishing Co., Amsterdam, 1963, pp. 93-194.
15. I. Weiss and S.L. Semiatin: *Mater. Sci. Eng.,* 1998, vol. A243, pp. 46-65.
16. I. Philippart and H.J. Rack: *Mater. Sci. Eng.,* 1998, vol. A243, pp. 196-200.
17. N.E.W. De Recca and C.M. Libanati: *Acta Metall.,* 1968, vol. 16 (10), pp. 1297-1305 (in French).
18. Z. Liu and G. Welsh: *Metall. Trans. A,* 1988, vol. 19A, pp. 1121-25.
19. J.F. Murdock, I.S. Lundy, and E.E. Stansbury: *Acta Metall.,* 1964, vol. 12 (9), pp. 1033-39.
20. M.L. Meir and A.K. Mukherjee: *Scripta Mater.,* 1991, vol. 25 (6), pp. 1471-76.
21. T. Seshacharyulu, S.C. Medeiros, W.G. Frazier, and Y.V.R.K. Prasad: *Mater. Sci. Eng.,* 2000, vol. A284, pp. 184-94.
22. I. Weiss and S.L. Semiatin: *Mater. Sci. Eng.,* 1999, vol. A 263, pp. 243-56.